Endoplasmic Reticulum Stress Drives Neuroinflammation Through Lipocalin 2 Upregulation in Retinal Microglia After Optic Nerve Injury

Weifeng Huang, Yaoming Liu, Jinmiao Li, Yang Gao, Junjie Tang, Siuhang Yip, Xinyue Wang, Hongwei Zhang, Yujun Ma, Shicai Su, Jiahe Nie, and Rong Lu

State Key Laboratory of Ophthalmology, Zhongshan Ophthalmic Center, Sun Yat-Sen University, Guangdong Provincial Key Laboratory of Ophthalmology Visual Science, Guangzhou, China

Correspondence: Rong Lu, State Key Laboratory of Ophthalmology, Zhongshan Ophthalmic Center, Sun Yat-Sen University, Guangdong Provincial Key Laboratory of Ophthalmology Visual Science, Guangzhou 510060, China; lurong@gzzoc.com.

Received: November 27, 2024
Accepted: April 12, 2025
Published: May 6, 2025

Citation: Huang W, Liu Y, Li J, et al. Endoplasmic reticulum stress drives neuroinflammation through lipocalin 2 upregulation in retinal microglia after optic nerve injury. *Invest Ophthalmol Vis Sci.* 2025;66(5):12. https://doi.org/10.1167/iovs.66.5.12

Purpose. This study aims to explore how lipocalin 2 (LCN2) connects endoplasmic reticulum (ER) stress and inflammation in optic nerve injury (ONI) and identify potential therapeutic strategies.

Methods. An optic nerve crush (ONC) mouse model was used to investigate the role of ER stress and LCN2 in ONI. Immunofluorescence, quantitative PCR, and Western blot analyses were performed to assess ER stress markers, LCN2, inflammation-related genes, and retinal ganglion cell (RGC) survival, with or without treatment of 4PBA (an ER stress inhibitor) and TUN (an ER stress activator) in both the ONC model and BV2 cells. *Lcn2* knockdown was achieved using small interfering RNA in BV2 cells and adeno-associated virus (AAV)–mediated gene silencing in vivo to explore underlying signaling pathways.

Results. ER stress markers (GRP78, ATF4, CHOP) and LCN2 expression were increased in ONC retinas, accompanied by microglial activation and RGC loss. Inhibition of ER stress using 4PBA effectively decreased LCN2 expression, attenuated microglial activation, and increased RGC survival post-ONC. Intravitreal injection of recombinant LCN2 induced a proinflammatory phenotype in microglia and exacerbated neurotoxicity. AAV-mediated *Lcn2* silencing mitigated microglial activation, reduced neuroinflammation, and provided RGC neuroprotection, surpassing 4PBA treatment. In vitro studies further confirmed that *Lcn2* knockdown significantly reduced the inflammatory response in BV2 cells by inhibiting NLRP3 inflammasome activation via the TLR4/NF-κB pathway.

Conclusions. This study elucidates the critical role of LCN2 in linking ER stress and inflammation in ONI, offering a promising therapeutic target. AAV-mediated *Lcn2* silencing outperforms broad ER stress inhibition, providing a novel strategy for treating optic nerve injuries.

Keywords: optic nerve injury, lipocalin 2, endoplasmic reticulum stress, 4-phenylbutyric acid, inflammation, retinal ganglion cells

Retinal ganglion cells (RGCs) are essential for transmitting visual information from the retina to the brain. Unfortunately, RGCs undergo progressive degeneration following optic nerve injury (ONI), resulting in irreversible vision loss, as seen in neurodegenerative conditions such as glaucoma and traumatic optic neuropathy.[1,2] The specific mechanisms underlying the loss of RGCs after ONI are still poorly understood, which limits the efficacy of current neuroprotective therapies.[3] Notably, endoplasmic reticulum (ER) stress–mediated cell death has emerged as a significant factor influencing postinjury RGC survival.[4]

ER stress serves as a defense mechanism against various forms of injury during the early stages. However, prolonged stress in the ER triggers the proapoptotic pathway and thereby exacerbates ER stress. This cascade ultimately leads to detrimental events such as inflammation, oxidative stress, and, ultimately, cell death.[5] Many studies have shown that ER stress–mediated cell death plays an important role in various neurodegeneration diseases, such as Parkinson disease,[6] Alzheimer disease,[7] amyotrophic lateral sclerosis,[8] glaucoma,[2,9] optic nerve injury,[10,11] and age-related macular degeneration,[12] and targeting ER stress holds promise as a therapeutic strategy for neuroprotection.[10,13] However, the molecular signaling of ER stress–induced cell death remains largely unclear.

Accumulating evidence indicates that the activated ER stress pathway is interconnected with various inflammatory pathways, contributing to the pathological processes of multiple diseases.[14,15] Prolonged ER stress acts as an inflammatory nidus, potentially triggering a defensive innate immune response to injury. Sustained overload of protein processing, induced by the release of numerous cytokines and chemokines during neuroinflammation, leads to excessive ER stress and creates a positive feedback loop that exacerbates injury.[16] Consequently, targeting these detrimental interactions between ER stress and neuroinflamma-

tion may provide therapeutic avenues for neurodegenerative diseases.

Lipocalin-2 (LCN2) is considered an acute-phase response protein in neuroinflammation following central nervous system (CNS) injury. It serves as a modulator of glial cell functional polarization, making it a potential target for mitigating proinflammatory activation and subsequent brain injury.[17,18] Previous studies utilizing RNA sequencing (RNA-seq) have observed significant alterations in LCN2 expression in an optic nerve crush (ONC) model, indicating its potential involvement in the loss of retinal ganglion cells.[19,20] Furthermore, previous clinical studies have implicated a strong correlation between increased LCN2 expression and ER stress in various diseases, including pulmonary disease,[21] cardiovascular disease,[22] kidney disease,[23] and neuronal degeneration disease.[24] These data suggest that LCN2 may participate in regulating ER stress and neuroinflammation, as well as ultimately impact the survival of RGCs following optic nerve injury, although its exact role remains uncertain at present.

Therefore, in this study, we aimed to elucidate the molecular mechanism by which LCN2 connects ER stress and inflammation in ONI, which may offer a promising therapeutic strategy for ONI treatment in the future.

Materials and Methods

Animals

All animals in this study were treated according to the ARVO statement on the Use of Animals in Ophthalmic and Vision Research. Experimental procedures were approved by the Institutional Animal Care and Use Committee of the Zhongshan Ophthalmic Center, adhering to the Guidelines for Animals in Research. Adult male C57BL/6 mice, aged 6 to 8 weeks, were obtained from the Animal Laboratory of the Zhongshan Ophthalmic Center (Guangzhou, China). The mice were housed under specific pathogen-free (SPF) conditions at 20°C to 25°C and 40% to 60% humidity, with a 12-hour light/dark cycle. Euthanasia was performed using increasing concentrations of CO_2 before retina extraction.

ONC Model

The classic model of ONC was conducted to induce optic nerve injury, following established protocols.[25] Briefly, mice were anesthetized by intraperitoneal injection of 1.25% 2,2,2-tribromoethanol (0.2 mL/10 g). The optic nerve was then carefully exposed and subjected to a 10-second crush, 1 mm posterior to the eyeball, using ultrafine self-closing forceps without damaging the blood vessels around the optic nerve. Only the left eye underwent ONC, with the contralateral, uninjured right eye serving as a control, as previously described.[26,27]

Pharmacologic Treatments in Animal Models

Adult mice were subjected to intravitreal injections using a WPI Nanofil syringe with a 35-gauge needle. After exposing the superior temporal side of anesthetized mice's eyes sufficiently while avoiding blood vessels, a slow injection into the vitreous cavity was carefully performed through the sclera 1 to 2 mm posterior to the corneoscleral limbus, ensuring minimal intraocular pressure elevation. For recombinant LCN2 (rLCN2, 1857-LC-050; R&D Systems, Minneapolis, MN, USA) treatment, the left eye of each mouse received 1 µg/mL rLCN2 in 1 µL of 0.01 M PBS immediately after ONC, while the right eye served as the control and received an equivalent volume of PBS alone. For adeno-associated virus (AAV)–mediated gene delivery, a separate cohort of mice received intravitreal injections of AAV2-U6-shLcn2-CMV-EGFP (AAV-Lcn2) and rAAV-U6-shRNA(scramble)-CMV-EGFP-SV40 pA (AAV2-EGFP) vectors (5.00×10^{12} vg/mL each). One minute after injection, the micropipette was carefully withdrawn to prevent leakage, and antibiotic ophthalmic ointment was applied to prevent infection. Additionally, eyes were monitored for signs of acute intraocular pressure elevation, such as corneal clouding, and no such sign was observed in any treated animals.

4-Phenylbutyric acid (4PBA, T5886; TargetMol, Boston, USA) was titrated to pH 7.4 with NaOH in sterile saline. Following ONC model establishment, mice in the 4PBA-treated group received 40 mg/kg (300 µL per injection), while the sham surgery group (naive eyes from untreated animals) was administered PBS at pH 7.4 (300 µL per injection). Both treatments were delivered intraperitoneally once daily.

Cell Lines and Culture Conditions

BV2 cells, a murine microglial cell line, were cultured in Dulbecco's modified Eagle's medium supplemented with 5% fetal bovine serum (Invitrogen, Carlsbad, CA, USA) and maintained in a 5% CO_2 incubator. Cells were treated with one or more of the following reagents: 4PBA (2.5 mM, T5886; TargetMol), a chemical chaperone and ER stress inhibitor, to investigate the role of ER stress in microglial activation and inflammatory responses; tunicamycin (TUN, 2 µg/mL, MB5419-1; Meilunbio, Dalian, China), a well-known inducer of ER stress, to establish an ER stress model and study its interplay with inflammation; or lipopolysaccharide (LPS, 1 µg/mL; Sigma Aldrich, St, Louis, MO, USA), a dual activator of inflammation and ER stress, to explore the relationship between ER stress and inflammatory responses.

Quantitative RT-PCR

At designated experimental time points, mice were euthanized, and their retinas were collected for RNA isolation using the EZ-press RNA Purification Kit (cat. B0004D; EZBioscience, Roseville, MN, USA). RNA purity and concentration were assessed using a Nanodrop 1000 spectrophotometer (Thermo Fisher Scientific, Waltham, MA, USA). cDNA synthesis was performed with 1000 ng total RNA using the EZBioscience 4× Reverse Transcription Master Mix (cat. A001GQ). The synthesized cDNA was included in a 10-µL reaction mixture for PCR amplification, which began with an initial denaturation at 95°C for 10 minutes, followed by 40 to 45 amplification cycles: denaturation at 95°C for 40 seconds, annealing at 53°C for 30 seconds, and extension at 72°C for 40 seconds (Roche, Basel, Switzerland). Relative transcription levels were quantified using the comparative Ct method, with Gapdh as an internal control. Primer sequences are provided in the Table.

RNA-Seq

A total of 2 µg RNA extracted from retinas using Trizol reagent (15596018; Invitrogen, USA) was utilized to generate a cDNA library according to Illumina's RNA-seq guidelines. This library was sequenced on an Illumina HiSeq2500 in a 2 × 150-bp paired-end format. Preprocessing with

Investigative Ophthalmology & Visual Science

Table. Primer Sequences Used for RT–qPCR

Gene	Forward (5′–3′)	Reverse (5′–3′)
Lcn2	GCAGGTGGTACGTTGTGGG	GCATTAGCTTCAGATTTACGGGT
Gapdh	AGGTCGGTGTGAACGGATTTG	TGTAGACCATGTAGTTGAGGTCA
Tnfa	GGTGCCTATGTCTCAGCCTCTT	GCCATAGAACTGATGAGAGGGAG
Il1b	TGGACCTTCCAGGATGAGGACA	GTTCATCTCGGAGCCTGTAGTG
Nos2	GAGACAGGGAAGTCTGAAGCAC	CCAGCAGTAGTTGCTCCTCTTC
Fcgr3	TGACAGTGGCTCCTACTTCTGC	GAGTCCTATCAGCAGGCAGAATG
Il6	TACCACTTCACAAGTCGGAGGC	CTGCAAGTGCATCATCGTTGTTC
Arg1	CATTGGCTTGCGAGACGTAGAC	GCTGAAGGTCTCTTCCATCACC
Ym1	TACTCACTTCCACAGGAGCAGG	CTCCAGTGTAGCCATCCTTAGG
Hspa5	TGTCTTCTCAGCATCAAGCAAGG	CCAACACTTCCTGGACAGGCTT
Atf4	AACCTCATGGGTTCTCCAGCGA	CTCCAACATCCAATCTGTCCCG
Ddit3	GGAGGTCCTGTCCTCAGATGAA	GCTCCTCTGTCAGCCAAGCTAG
Ppp1r15a	GGCGGCTCAGATTGTTCAAAGC	CCAGACAGCAAGGAAATGGACTG

Trimmomatic (Version 0.36; http://www.usadellab.org/cms/?page=trimmomatic) eliminated low-quality and adapter-contaminated reads. High-quality reads were aligned to the mouse genome (mm10) using HISAT2 (v.2.1.0; https://daehwankimlab.github.io/hisat2), with the genome obtained from Ensembl's FTP. Gene expression was quantified using uniquely mapped reads and feature counts based on Ensembl's mouse gene annotations. Log_2-transformed fold changes (LogFC) and differentially expressed genes were identified using DESeq2 after TMM (Trimmed Mean of M-values) normalization (FDR < 0.01, $|\text{LogFC}| > 3$) to control the false discovery rate (FDR). Gene Ontology (GO) and Kyoto Encyclopedia of Genes and Genomes (KEGG) analyses were performed using R to elucidate the functional enrichment and signaling pathways associated with down-regulated genes between the LPS-treated group and the LPS + 4PBA-treated group ($n = 3$).

In Vitro Cell Transfection

Small interfering RNA (siRNA) targeting *Lcn2* was obtained from Genepharma (Shanghai, China), including si*Lcn2*-1 (Sense: 5′-GGCAGCUUUACGAUGUACATT-3′; Antisense: 5′-UGUACAUCGUAAAGCUGCCTT-3′), si*Lcn2*-2 (Sense: 5′-GCUACUGGAUCAGAACAUUTT-3′; Antisense: 5′-AAUGUU CUGAUCCAGUAGCTT-3′), si*Lcn2*-3 (Sense: 5′-GCCUCAA GGACGACAACAUTT-3′; Antisense: 5′-AUGUUGUCGUCCUU GAGGCTT-3′), and si*Lcn2*-4 (Sense: 5′-CCACCAUACCAAG GAGCAUTT-3′; Antisense: 5′-AUGUUGUCGUCCUUGAGGCT T-3′). A negative control siRNA (si-Negative) was also included. BV2 cells were cultured in complete medium in 6-well plates for 24 hours. Transfections were performed with 100 nM siRNA using HiPerFect reagent (301704; Qiagen, Venlo, Netherlands), following the manufacturer's protocol. After 24 hours, transfected cells were exposed to LPS for 24 hours before Western blotting and further analysis.

Western Blotting

Mouse retinas and BV2 cells were homogenized in RIPA lysis buffer containing a protease inhibitor cocktail, phenylmethylsulfonyl fluoride (PMSF), and phosphatase inhibitors. Protein concentration was quantified using the BCA protein assay kit (Thermo Fisher Scientific). Western blotting was performed according to established protocols,[28] utilizing specific antibodies: LCN2 (1:800, AF1857; R&D Systems, Minneapolis, MN, USA), Iba1 (1:500, ab178846; Abcam, Cambridge, UK), GRP78 (1:800, AF5366; Affinity Biosciences, Cincinnati, OH, USA), ATF4 (1:800, DF6008; Affinity Biosciences), CHOP (1:800, AF6277; Affinity Biosciences), iNOS (1:800, ab178945; Abcam), IL-1β (1:800, AF5103; Affinity Biosciences), TLR4 (1:800, #40697; Signalway Antibody, Greenbelt, MD, USA), NF-κB (1:800, #6956; CST, Danvers, MA, USA), p-NF-κB (1:800, #3033; CST), NLRP3 (1:800, #DF7438; Affinity Biosciences), Lamin B1 (1:800, AF5161; Affinity Biosciences), and β-tubulin (1:10,000, HC101-02; Transgen Biotech, Beijing, China). Blots were incubated with horseradish peroxidase (HRP)–conjugated secondary antibodies for 2 hours at room temperature, followed by three 10-minute washes with Tris-buffered saline containing 0.1% Tween-20. Visualization was conducted using enhanced chemiluminescence (Tanon, Shanghai, China) and captured with the Tanon 5200 Multi-Image System.

Whole–Mounted Retinal Immunofluorescence

Retinas were fixed in 4% paraformaldehyde (PFA) at room temperature for 1 hour and then dissected into whole mounts. Four radial incisions (superior, inferior, temporal, nasal) were made to shape the retinas into a "petal." The retinas were washed three times for 10 minutes with PBST (G2157-1L; Servicebio, Wuhan, China) on a shaker, then blocked with Quickblock (P0260; Beyotime, Shanghai, China) for 15 minutes. They were incubated overnight at 4°C with the primary antibody against the RGC-specific marker RNA Binding Protein with Multiple Splicing (RBPMS, rabbit, 1:200, GTX118619; GeneTex, Irvine, California, USA). After extensive washing with PBST, Alexa Fluor 594–conjugated secondary antibodies (A11012; ThermoFisher, Waltham, Massachusetts, USA) were applied and incubated at room temperature for 2 hours. The retinas were washed again three times with PBST for 10 minutes on a shaker. Stained tissues were flat-mounted on glass slides with an antifluorescence quenching agent and covered with coverslips. Four areas (0.4 × 0.4 mm) from the center of each quadrant of the retina were photographed. RGCs were counted, and their survival rate was estimated using ImageJ software (National Institutes of Health, Bethesda, MD, USA).

Immunofluorescence Staining and Immunohistochemistry of Retinal Sections

Eyes were fixed overnight at 4°C in eyeball fixative solution (B0006; Powerful Biology, Wuhan, China), embedded in

Investigative Ophthalmology & Visual Science

paraffin, and sectioned horizontally into 4-µm slices through the optic nerve head. For immunofluorescence, sections were dewaxed, subjected to high-pressure antigen retrieval, blocked with goat serum for 1 hour at room temperature, and incubated overnight at 4°C with primary antibodies: LCN2 (1:200, AF1857; R&D Systems), Iba1 (1:200, ab178846; Abcam), GFAP (1:100, AF2594; R&D Systems), and Tuj1 (1:250, 801202; BioLegend, San Diego, California, USA). Sections were subsequently treated with Alexa Fluor 488/594–conjugated secondary antibodies (1:500; Abcam) for 2 hours at room temperature and counterstained with DAPI. Images were captured using a confocal microscope (LSM880; Zeiss, Oberkochen, Germany) with a 20× objective.

Cells were cultured on poly-D-lysine (Sigma)–coated coverslips, fixed with 4% paraformaldehyde for 15 minutes, and treated with 0.2% Triton X-100 for 10 minutes at 37°C. After blocking with 5% bovine serum albumin for 30 minutes, samples were incubated with NF-κB antibody (1:400, #6956; CST) and subsequently treated with Alexa Fluor 594–conjugated secondary antibody (1:500; Abcam). Nuclei were stained using DAPI-containing mounting medium (ab104139; Abcam).

For immunohistochemistry, sections were deparaffinized, rehydrated, and treated with 0.3% H_2O_2 in methanol to inhibit endogenous peroxidase activity. Following a 30-minute incubation with 5% bovine serum albumin, sections were incubated overnight at 4°C with primary antibodies against LCN2 (1:150, AF1857; R&D Systems). After washing with PBS, sections were treated with HRP-conjugated secondary antibodies for 1 hour at room temperature. Specimens were developed with diaminobenzidine, counterstained with hematoxylin, dehydrated through gradient ethanol, and cleared in xylene. Samples were visualized with a light microscope (Eclipse ci; Nikon, Tokyo, Japan) using a 40× objective.

Optical Coherence Tomography

Two weeks post-ONC modeling, optical coherence tomography (OCT) was performed using a Spectralis HRA + OCT + Multicolor system (Heidelberg Engineering, Heidelberg, Germany), following a circular scan protocol centered on the optic nerve head. Mice were anesthetized and their pupils dilated before being placed in front of the camera for retinal scanning. The thicknesses of the nerve fiber layer, ganglion cell layer, and inner plexiform layer were measured and summed to determine the inner retinal layer thickness. Measurements were conducted by a skilled technician, capturing 100 overlapping images per session, and retinal nerve fiber layer thickness was analyzed using ImageJ software.

Statistical Analysis

Statistical analysis was performed using GraphPad version 8.0.2 (GraphPad Software, La Jolla, CA, USA), with data expressed as mean ± SEM. Both Student's *t*-test and one-way ANOVA with Tukey's post hoc test were employed for the evaluations. All experimental procedures were independently repeated with sample sizes greater than or equal to 3 ($n \geq 3$). Statistical significance was established at a P value threshold of 0.05 or lower, with exact significance levels indicated in the corresponding figures.

Results

ER Stress Precedes Microglial Activation and RGC Degeneration Following ONC

To delineate the temporal progression of pathological events after ONC, we systematically analyzed retinal responses at critical postinjury time points. Retinal ganglion cell (RGC) quantification via RBPMS immunofluorescence revealed preserved RGC density at day 3 (93.8% ± 6.6% of sham controls, $P = 0.384$), followed by progressive degeneration at day 5 (52.1% ± 7.0%, $P < 0.001$) and day 7 (29.9% ± 6.0%, $P < 0.0001$) post-ONC (Figs. 1A, 1B). Molecular profiling identified ER stress induction preceding RGC loss, with quantitative RT-PCR (RT-qPCR) demonstrating significant upregulation of ER stress markers *Hspa5* (also known as GRP78), *Atf4*, and *Ddit3* (also known as CHOP) as early as 4 hours postinjury (Figs. 1C–E). Immunofluorescence confirmed sustained GRP78 protein elevation (1.9-fold increase vs. sham, $P < 0.001$) by day 3, with dual staining localizing GRP78 upregulation specifically within $Iba1^+$ microglia (Figs. 1F–G), implicating microglial ER stress in early pathogenesis. Concomitantly, at this 3-day time point, microglial activation became evident through a 68.3% increase in $Iba1^+$ cell density ($P < 0.01$) and a 2.41-fold rise in $CD68^+/Iba1^+$ ratio ($P < 0.001$), indicating phagocytic activation (Figs. 1H–J). Importantly, retinal neuroinflammation exhibited delayed initiation relative to ER stress: transcriptional upregulation of *Nos2* and *Il1b* began at 8 hours postinjury, peaked at day 3, and persisted through day 7 (Figs. 1K, 1L).

This temporal profiling reveals a sequential cascade: ER stress induction → microglial activation → RGC degeneration. The spatial overlap of GRP78 with activated microglia suggests ER stress may directly drive neuroinflammatory responses, positioning microglial ER stress as a potential therapeutic target to disrupt the degenerative cascade.

Inhibiting ONC-Induced ER Stress With 4PBA Alleviates Microglial Activation, Promotes RGC Survival, and Preserves Retinal Structure

To investigate the therapeutic potential of ER stress modulation, 4PBA was administered intraperitoneally daily in ONC-injured mice. RT-PCR analysis of ER stress–related genes (Atf4, *Ddit3* [CHOP], *Ppp1r15a* [GADD34], and *Hspa5* [GRP78]) at 7 days post-ONC demonstrated significant ER stress activation in injured retinas, which was effectively suppressed by 4PBA treatment (Fig. 2A). Immunoblotting revealed elevated CHOP and GRP78 protein levels in ONC retinas compared to uninjured controls, with a marked reduction in 4PBA-treated versus PBS controls (Figs. 2B, 2C), confirming pharmacologic ER stress attenuation.

Building on the observed microglial ER stress in Figure 1, we assessed microglial responses through Iba1 immunostaining of retinal flat mounts. 4PBA treatment significantly reduced microglial density (30.7% decrease vs. PBS, $P < 0.01$) and a morphologic transition from activated amoeboid to resting ramified states (Figs. 2D, 2E). Consistent with this phenotypic shift, IL-1β and iNOS protein expression were also downregulated in 4PBA-treated retinas (Fig. 2F).

RGC survival analysis demonstrated progressive neuroprotection by 4PBA. At 1-week post-ONC, 4PBA-treated

Investigative Ophthalmology & Visual Science

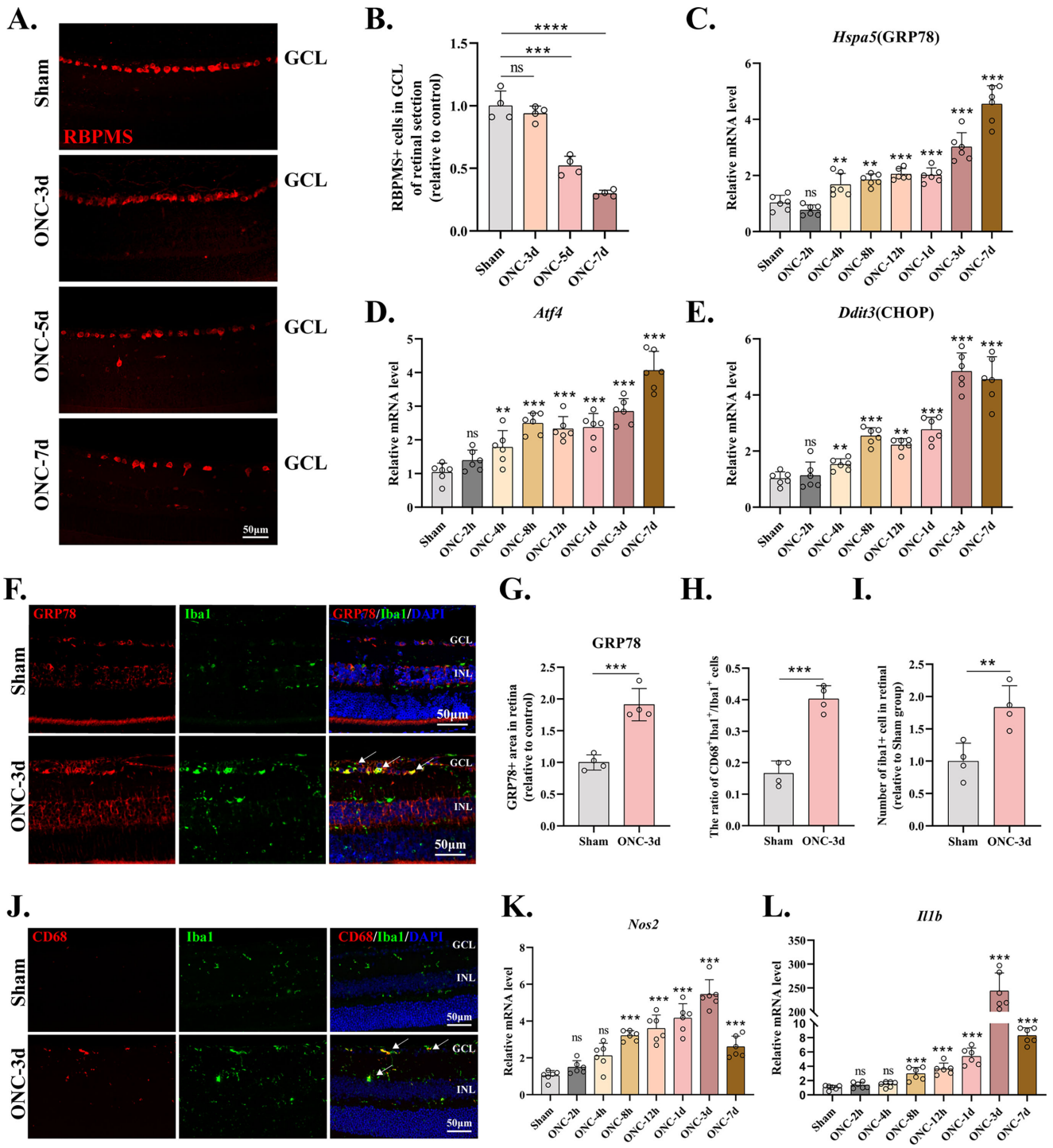

Figure 1. ER stress precedes retinal ganglion cell loss and microglial activation following ONC. (**A**, **B**) RGC survival analysis by RBPMS immunofluorescence. (**A**) Representative images of a retinal ganglion cell layer (GCL) from sham-operated controls and at 3, 5, and 7 days post-ONC. *Scale bar*: 50 µm. (**B**) Quantification of RBPMS$^+$ cells expressed as a percentage of sham control. Data represent mean ± SEM ($n = 4$ biological replicates). ns, not significant. ***$P < 0.001$, ****$P < 0.0001$ (unpaired *t*-test). (**C–E**) ER stress marker mRNA expression. RT-qPCR analysis of (**C**) *Atf4*, (**D**) *Ddit3* (CHOP), and (**E**) *Hspa5* (GRP78) at indicated time points post-ONC. Data normalized to sham controls (mean ± SEM, $n = 6$). *$P < 0.001$, **$P < 0.01$, ****$P < 0.0001$ (unpaired *t*-test). (**F–G**) Spatial localization of ER stress. (**F**) Dual immunofluorescence of GRP78 and Iba1$^+$ microglia in retinal cross sections at day 3 post-ONC. *Scale bar*: 50 µm. (**G**) Quantification of GRP78$^+$ area normalized to sham. Data represent mean ± SEM ($n = 4$). *$P < 0.001$ (unpaired *t*-test). (**H–J**) Phagocytic microglial activation. (**H**) CD68$^+$/Iba1$^+$ ratio. (**I**) Iba1$^+$ cell density in the retinal. (**J**) Representative Iba1/CD68 costaining images at day 3 post-ONC. *Scale bar*: 50 µm. (**I**) Iba1$^+$ cell density in the retinal. (**H**) CD68$^+$/Iba1$^+$ ratio. Data: mean ± SEM ($n = 4$). **$P < 0.01$, ***$P < 0.001$ (unpaired *t*-test). (**K–L**) Neuroinflammatory gene expression. RT-qPCR analysis of (**K**) *Nos2* and (**L**) *Il1b* across post-ONC time course. Data normalized to sham (mean ± SEM, $n = 6$). *$P < 0.001$, ****$P < 0.0001$ (unpaired *t*-test).

Investigative Ophthalmology & Visual Science

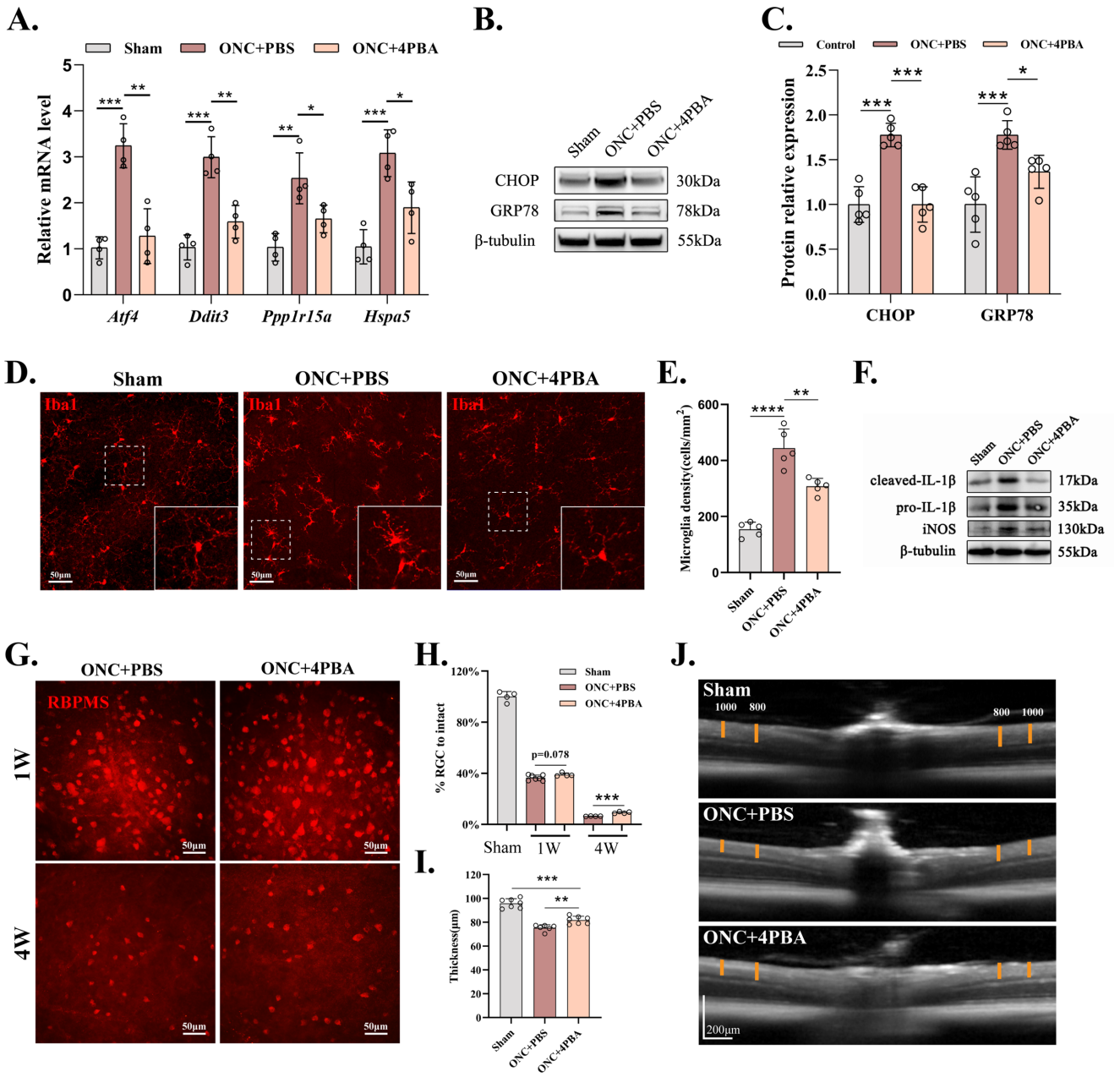

Figure 2. Inhibiting ONC-induced ER stress with 4PBA alleviates microglial activation, promotes RGC survival, and preserves retinal structure. (**A**) RT-qPCR analysis of ER stress–related genes (*Atf4*, *Ddit3* [CHOP], *Ppp1r15a* [GADD34], and *Hspa5* [GRP78]) demonstrates significant mRNA elevation in ONC + PBS retinas versus the ONC + 4PBA group. Data: mean ± SEM (n = 4–6). $P < 0.05$, *$P < 0.01$, **$P < 0.001$, ***$P < 0.0001$ (one-way ANOVA). (**B**, **C**) Western blot quantification shows 4PBA-mediated reduction of CHOP and GRP78 protein levels in ONC retinas compared to PBS controls. Data: mean ± SEM (n = 5). $P < 0.05$, *$P < 0.01$, **$P < 0.001$ (one-way ANOVA). (**D**, **E**) Iba1$^+$ microglial activation analysis by retinal whole-mount immunofluorescence. 4PBA treatment significantly reduces microglia density (30.7% decrease vs. PBS) and promotes ramified morphology. Data: mean ± SEM (n = 5). *$P < 0.01$, ***$P < 0.0001$ (one-way ANOVA). *Scale bar*: 50 μm. (**F**) Western blot analysis confirms downregulation of pro–IL-1β, cleaved IL-1β, and iNOS protein expression in 4PBA-treated versus PBS-treated ONC retinas. (**G**, **H**) RBPMS$^+$ retinal ganglion cell survival assessment by whole-mount immunofluorescence. 4PBA treatment mitigates RGC loss compared to PBS controls. Data: mean ± SD ($n \geq 4$). **$P < 0.001$. *Scale bar*: 50 μm. (**I**, **J**) Representative image of retinal thickness determined by OCT in the sham, ONC + PBS, and ONC + 4PBA groups. Two vertical calipers were placed on each side of the optic nerve head, 800 and 1000 μm away from the center of the optic nerve head. The combined thickness (μm) of the nerve fiber layer, ganglion cell layer, and inner plexiform layer was measured. The ONC + 4PBA group exhibited significantly less thinning compared to the ONC + PBS group. For each treatment group, $n \geq 3$. Data are presented as mean ± SD. **$P < 0.01$, ***$P < 0.001$.

retinas showed a numerical improvement in RBPMS$^+$ cell survival (38.9% ± 4.7% of uninjured controls) compared to PBS-treated animals (36.5% ± 5.2%, $P = 0.187$), suggesting early therapeutic potential. This trend toward preservation became statistically significant by 4 weeks, with PBS controls exhibiting catastrophic neuronal loss (6.4% ± 2.1% survival vs. uninjured controls) compared to substantially rescued RGC populations in 4PBA-treated retinas (9.3% ± 1.8%,

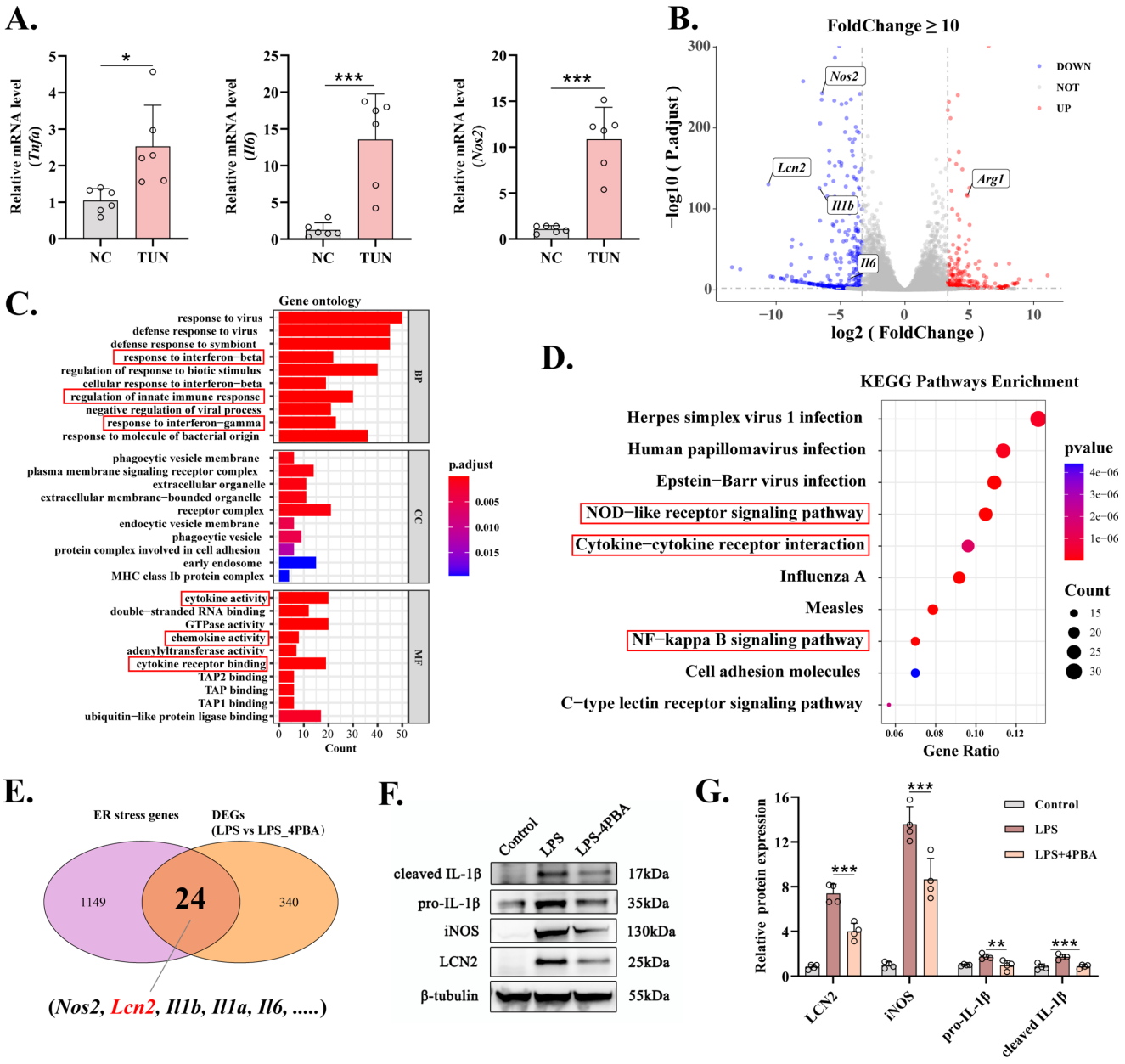

Figure 3. Inhibiting ER stress with 4PBA alleviates inflammation in BV2 cells in vitro. (**A**) RT-qPCR analysis of *Tnfa*, *Il6*, and *Nos2* mRNA levels in TUN-treated BV2 cells reveals ER stress–induced proinflammatory activation versus untreated controls (NC). Data: mean ± SEM ($n = 6$). $P < 0.05$, $^{**}P < 0.001$ (Student's *t*-test). (**B**) Volcano plot illustrating downregulation of mRNA expression associated with proinflammatory responses in BV2 cells treated with 4PBA under LPS-induced inflammatory conditions, as assessed through bulk RNA-seq analysis. (**C**) GO analysis of the downregulated differentially expressed genes (DEGs) between the LPS group and LPS + 4PBA group in BV2 cells. (**D**) KEGG pathway analysis confirms suppression of LPS-induced inflammatory cascades, including NOD-like receptor and NF-κB signaling (top 15 pathways shown). (**E**) Intersection analysis identifies 24 shared genes between ER stress–associated genes (GeneCards) and LPS_4PBA DEGs, including key mediators *Nos2*, *Lcn2*, *Il1b*, and *Il6*. (**F**, **G**) Western blot quantification demonstrates 4PBA-mediated downregulation of LCN2, pro–IL-1β, cleaved IL-1β, and iNOS protein levels versus LPS controls. Data: mean ± SEM ($n = 4$). $P < 0.05$, $^{**}P < 0.001$ (one-way ANOVA).

$P < 0.001$ vs. PBS; Figs. 2G, 2H). Structural assessment via OCT at day 14 corroborated these findings, showing substantial thinning of inner retinal layers (nerve fiber layer + ganglion cell layer + inner plexiform layer) in PBS controls (versus uninjured, $P < 0.001$), which was significantly mitigated by 4PBA treatment ($P < 0.01$ vs. PBS; Figs. 2I, 2J). These findings demonstrate that 4PBA-mediated ER stress inhibition attenuates microglial activation, enhances RGC survival, and preserves retinal structural integrity following ONC.

Inhibiting ER Stress With 4PBA Alleviates Inflammation in BV2 Cells In Vitro

To investigate ER stress–inflammation crosstalk in microglia, we utilized BV2 murine microglial cells. RT-PCR analysis demonstrated that tunicamycin-induced ER stress significantly upregulated proinflammatory factors *Tnfa*, *Il6*, and *Nos2* (Fig. 3A), mirroring our in vivo observations. Given the well-documented capacity of LPS to induce concurrent inflammation and ER stress,[16,29] we conducted bulk RNA

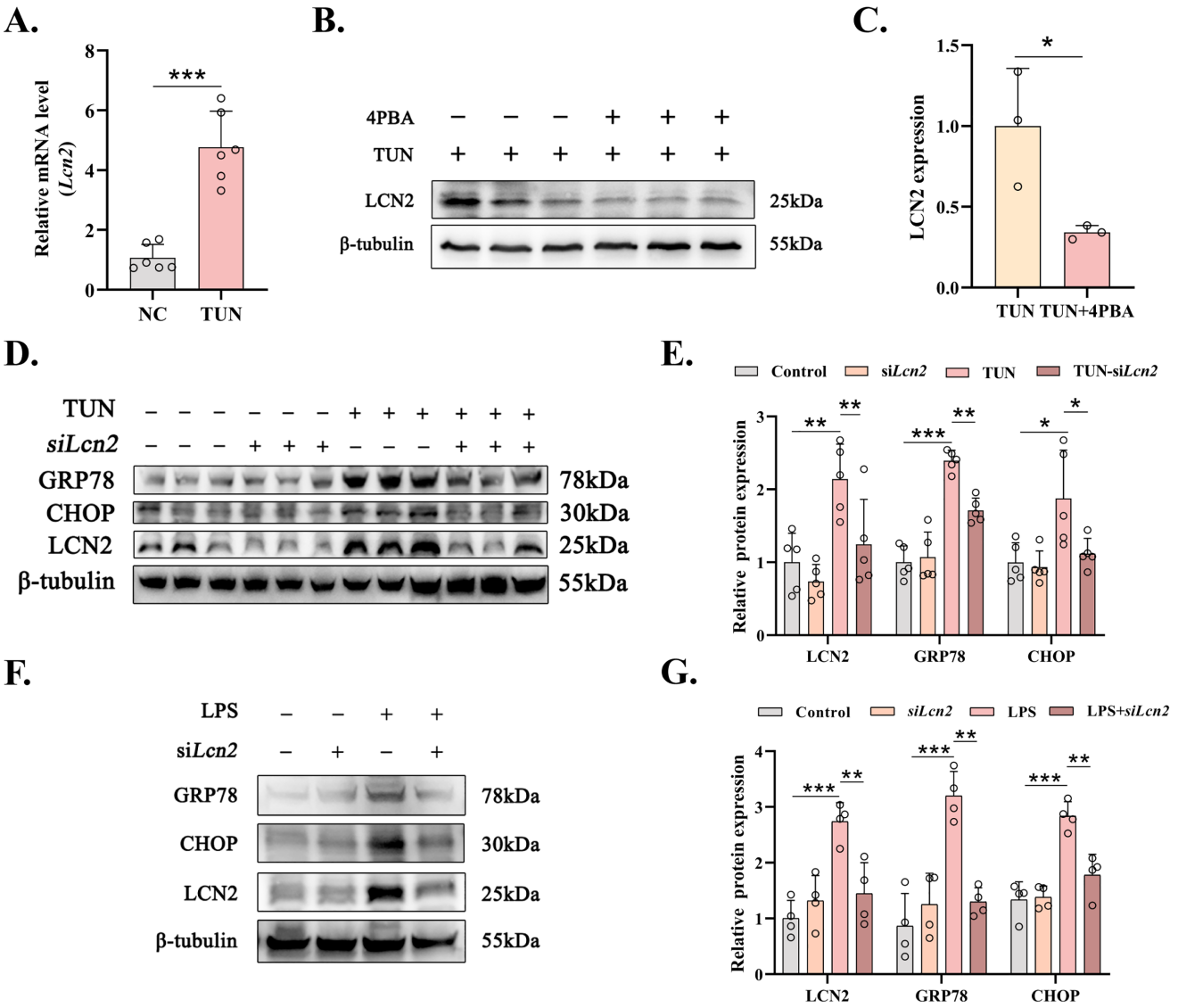

Figure 4. Mutual promotion between LCN2 and ER stress. (**A**) RT-qPCR results indicate elevated mRNA levels of *Lcn2* in the TUN group compared to the NC group. Data are shown as mean ± SEM with $n = 6$ biological repeats. $^{***}P < 0.001$, calculated by Student's *t*-test. (**B**, **C**) Immunoblot analysis demonstrates a significant decrease in LCN2 protein expression in the TUN + 4PBA group compared to the TUN group in BV2 cells. Data are shown as mean ± SEM with $n = 4$. $^{*}P < 0.05$, $^{***}P < 0.001$, calculated by Student's *t*-test. (**D**, **E**) Immunoblot analysis shows a significant upregulation of GRP78 and CHOP protein expression in the TUN group compared to the negative control group in BV2 cells, which was alleviated by *Lcn2* knockdown using siRNA. Data are shown as mean ± SEM with $n = 5$. $^{*}P < 0.05$, $^{**}P < 0.01$, $^{***}P < 0.001$, calculated by one-way ANOVA. (**F**, **G**) Immunoblot analysis shows a significant upregulation of GRP78 and CHOP protein expression in the LPS group compared to the negative control group in BV2 cells, which was alleviated by *Lcn2* knockdown using siRNA. Data are shown as mean ± SEM with $n = 4$. $^{**}P < 0.01$, $^{***}P < 0.001$, calculated by one-way ANOVA.

sequencing following LPS stimulation to dissect ER stress–dependent inflammatory cascades. Transcriptomic profiling revealed 4PBA-mediated suppression of key inflammatory mediators (*Nos2*, *Il1b*, and *Il6*; Fig. 3B).

GO analysis of significantly downregulated genes (LogFC > 3, *P*adj < 0.05) identified enriched biological processes, including interferon-beta/gamma response and innate immune regulation, with molecular functions centered on cytokine/chemokine activity and receptor binding (Fig. 3C). KEGG pathway analysis further demonstrated 4PBA-induced attenuation of LPS-activated pathways: NOD-like receptor signaling, NF-κB cascade, cytokine–cytokine receptor interaction, and Toll-like receptor signaling (Fig. 3D).

Intersectional analysis of LPS_4PBA versus LPS differentially expressed genes with ER stress–associated genes from GeneCards identified 24 shared regulators, including *Nos2*, *Lcn2*, *Il1b*, *IL-1a*, and *Il6* (Fig. 3E). Immunoblot validation confirmed 4PBA-induced downregulation of cleaved IL-1β, pro-IL-1β, iNOS, and LCN2 proteins (Figs. 3F, 2G). Notably, given LCN2's established role in neuroinflammation propagation and neuronal death,[17,18] these findings position it as a critical node linking ER stress with inflammatory cascades, requiring mechanistic interrogation. This molecular nexus provides the foundation for our subsequent investigation into LCN2's specific contributions to ER stress–driven retinal degeneration.

Investigative Ophthalmology & Visual Science

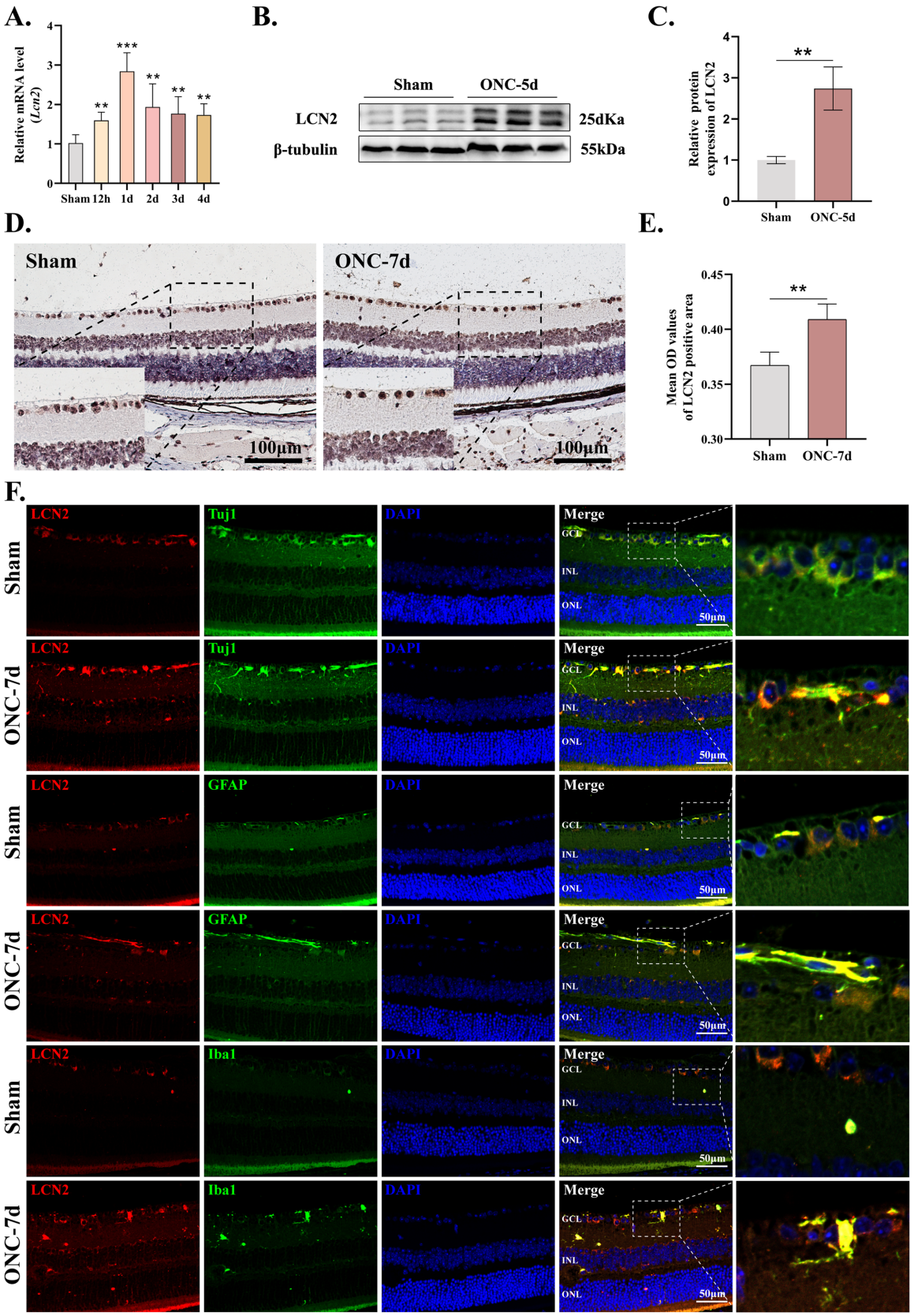

Figure 5. Upregulation of LCN2 expression in the retina post-ONC. (**A**) RT-qPCR results indicate elevated mRNA levels of *Lcn2* in the ONC group compared to the sham group. Data are shown as mean ± SEM with $n = 5$ biological repeats. ***$P < 0.001$, calculated by Student's *t*-test. (**B**, **C**) Immunoblot analysis demonstrates a significant increase in LCN2 expression in the retina in the ONC group compared to the sham group. Data are shown as mean ± SEM with $n = 3$. **$P < 0.01$, calculated by Student's *t*-test. (**D**, **E**) Immunohistochemical analysis shows an increase in LCN2 expression in the retina following ONC. Data are shown as mean ± SEM with $n = 4$–5 biological repeats. **$P < 0.01$, calculated by Student's *t*-test. (**F**) Immunofluorescence analysis reveals LCN2 (*red*) predominantly localized to Tuj1$^+$ RGCs in sham retinas. Following ONC injury, prominent LCN2 accumulation is observed in Iba1$^+$ microglia and GFAP$^+$ astrocytes. *Scale bar*: 50 μm.

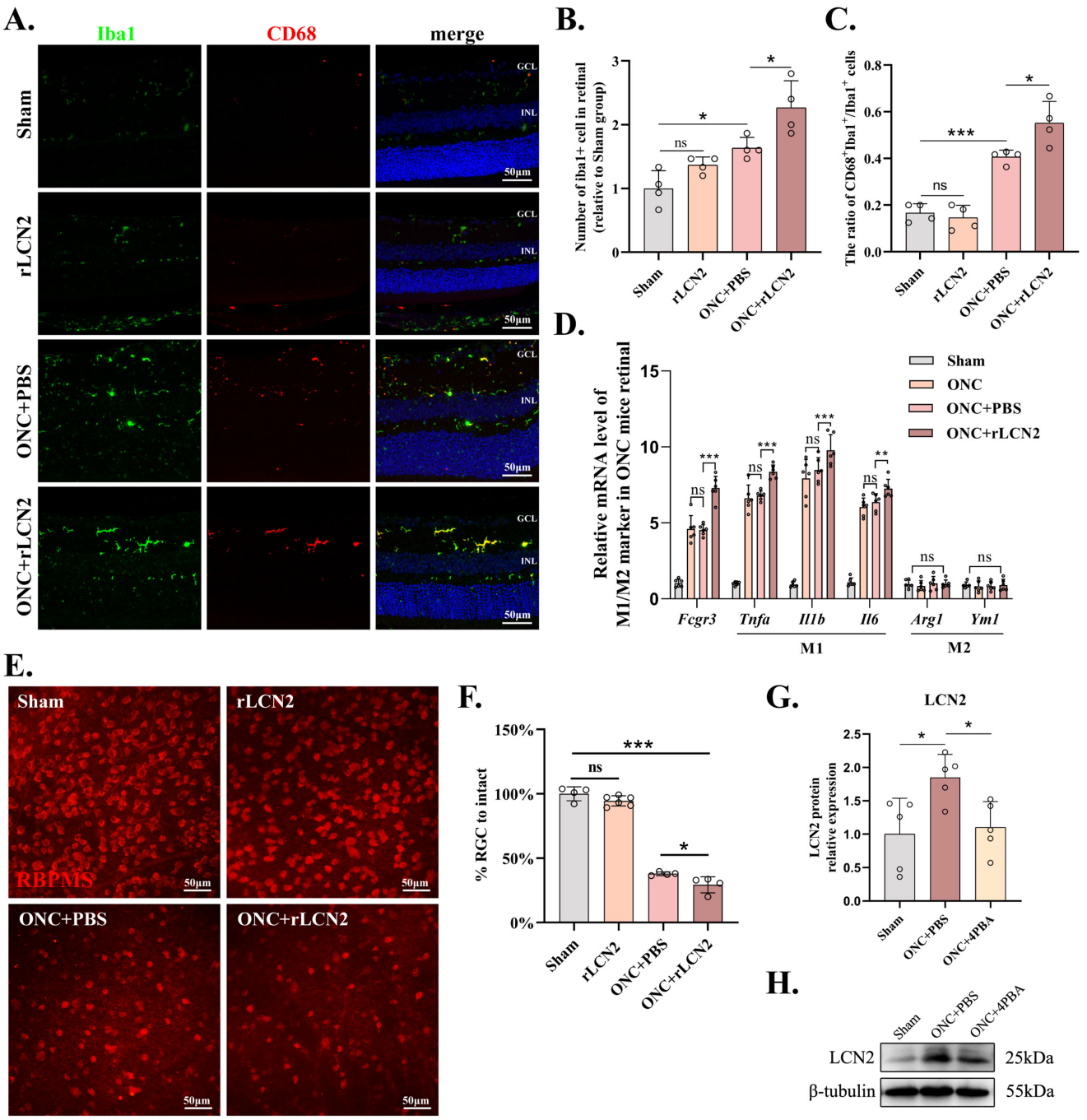

Figure 6. LCN2 exacerbates neuroinflammation and retinal ganglion cell degeneration post-ONC. (**A–C**) Microglial phagocytic activation in retinal flat mounts visualized by $CD68^+/Iba1^+$ dual immunofluorescence across experimental groups at 7 days post-ONC. *Scale bar*: 50 μm. Quantification of (**B**) $Iba1^+$ cell density and (**C**) $CD68^+/Iba1^+$ activation index. Data represent mean ± SEM; $n = 4$ biological replicates; $^*P < 0.05$, $^{***}P < 0.001$ (one-way ANOVA with Tukey's post hoc test). (**D**) Transcriptional profiling of microglial-associated inflammatory mediators in retinal tissues. RT-qPCR analysis of *Fcgr3*, *Tnfa*, *Il1b*, and *Il6* mRNA levels normalized to *Gapdh*. Data represent mean ± SEM; $n = 6$; $^{**}P < 0.01$, $^{***}P < 0.001$ (one-way ANOVA with Tukey's post hoc test). (**E**, **F**) RGC degeneration quantification by $RBPMS^+$ cell counting in retinal whole mounts. (**E**) Representative images showing RGC loss patterns. (**F**) Survival rates normalized to sham controls. *Scale bars*: 50 μm. Data represent mean ± SEM; $n = 4$–6; $^*P < 0.05$, $^{***}P < 0.001$ (one-way ANOVA with Tukey's post hoc test). (**G**, **H**) Therapeutic modulation of LCN2 by 4PBA treatment. (**G**) Quantification of LCN2 protein levels normalized to β-tubulin and (**H**) representative immunoblots. Data represent mean ± SEM; $^*P < 0.05$, calculated by one-way ANOVA.

LCN2 Is Mutually Promotive With ER Stress and Participates in ER Stress Regulation

Given the strong association between LCN2 expression and ER stress, further investigation was conducted to explore their dynamic interactions. BV2 cells were treated with TUN to induce ER stress, and RT-PCR analysis revealed a significant upregulation *Lcn2* mRNA level versus untreated controls ($P < 0.001$; Fig. 4A). Immunoblotting confirmed this upregulation, which was mitigated by 4PBA treatment (Figs. 4B, 4C), establishing ER stress as a key driver of LCN2 expression.

Investigative Ophthalmology & Visual Science

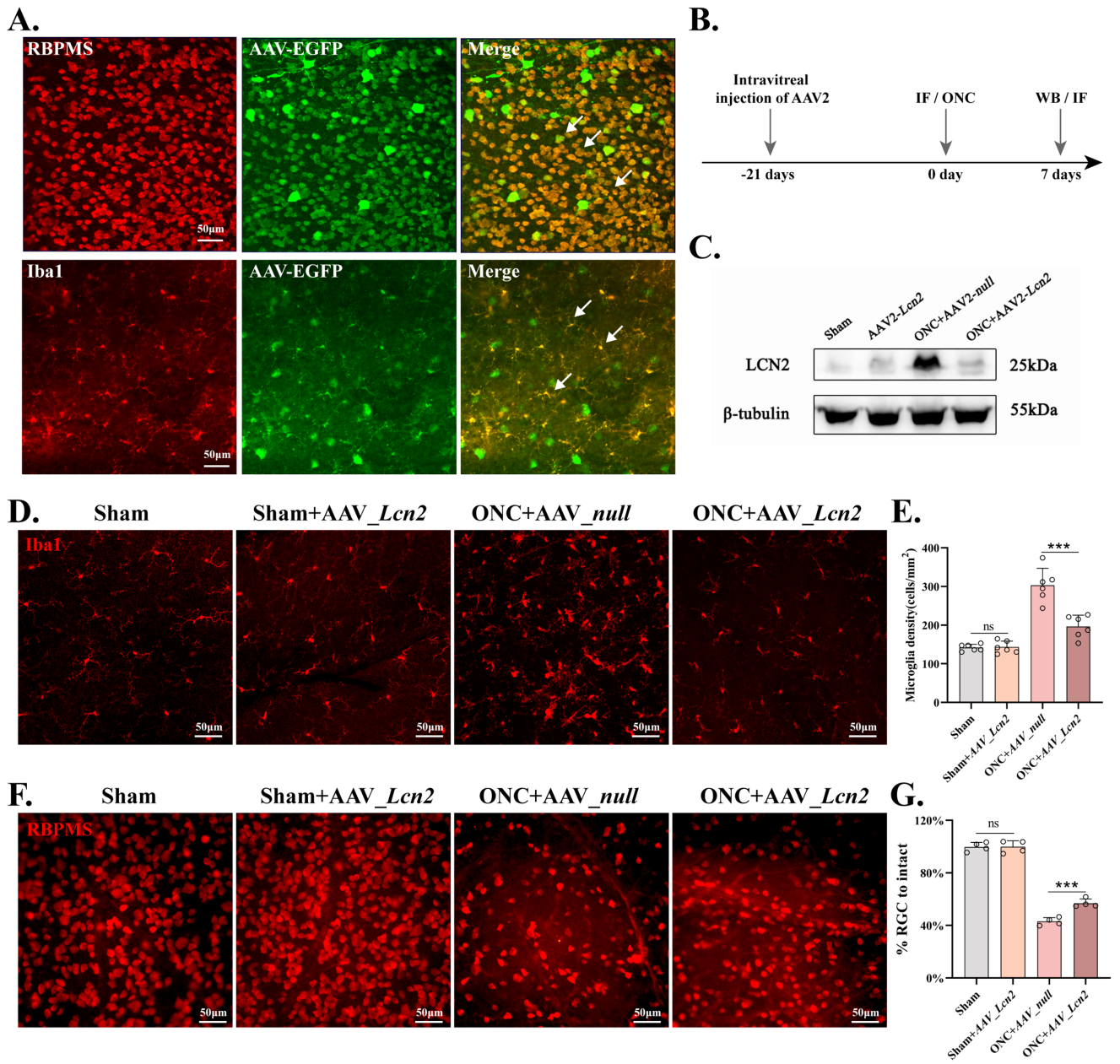

Figure 7. AAV-mediated LCN2 gene silencing reduces microglial activation and enhances RGC survival following ONC. (**A**, **B**) Retinal whole mounts at 3 weeks after intravitreal injection of AAV2-U6-shLcn2-CMV-EGFP (AAV-Lcn2) demonstrate EGFP fluorescence (*green*) colocalized with RBPMS$^+$ RGCs (*red*) and Iba1$^+$ microglia (*red*), confirming targeted delivery to both RGCs and microglia. *Scale bars*: 50 µm. (**C**) Western blot shows markedly reduced LCN2 protein levels in ONC-injured retinas treated with AAV-Lcn2 versus AAV-null controls. (**D**, **E**) AAV-Lcn2 treatment reduces microglial density by 35.2% in ONC-injured retinas, accompanied by a morphologic shift from amoeboid to ramified states. *Scale bars*: 50 µm. Data represent mean ± SEM; $n = 4$; ***$P < 0.001$ (one-way ANOVA with Tukey's post hoc test). (**F**, **G**) Lcn2 silencing elevates RGC survival to 53.5% ± 3.1% post-ONC, significantly exceeding AAV-null controls (40.5% ± 2.8%; $P < 0.001$). *Scale bars*: 50 µm. Data: mean ± SEM; $n = 4$; *$P < 0.001$ (one-way ANOVA, Tukey's post hoc test).

To determine whether LCN2 reciprocally modulates ER stress, *Lcn2* was silenced via siRNA. Remarkably, *Lcn2* depletion in TUN-stimulated BV2 cells reduced CHOP ($P < 0.05$) and GRP78 ($P < 0.01$) protein levels compared to the TUN-alone group (Figs. 4D, 4E). This reciprocal modulation extended to LPS-induced models, where *Lcn2* depletion suppressed LPS-driven CHOP ($P < 0.01$) and GRP78 ($P < 0.01$) upregulation (Figs. 4F, 4G), demonstrating conserved regulation across distinct ER stress triggers. These findings establish a self-reinforcing cycle: ER stress elevates LCN2 expression, which in turn potentiates ER stress signaling through CHOP/GRP78 activation. This pathogenic feedforward loop provides a mechanistic rationale for targeting LCN2–ER stress crosstalk in neuroinflammatory disorders.

Upregulation of LCN2 Expression Following ONC

To delineate the injury-responsive dynamics of LCN2 in vivo, we performed longitudinal profiling of LCN2 expres-

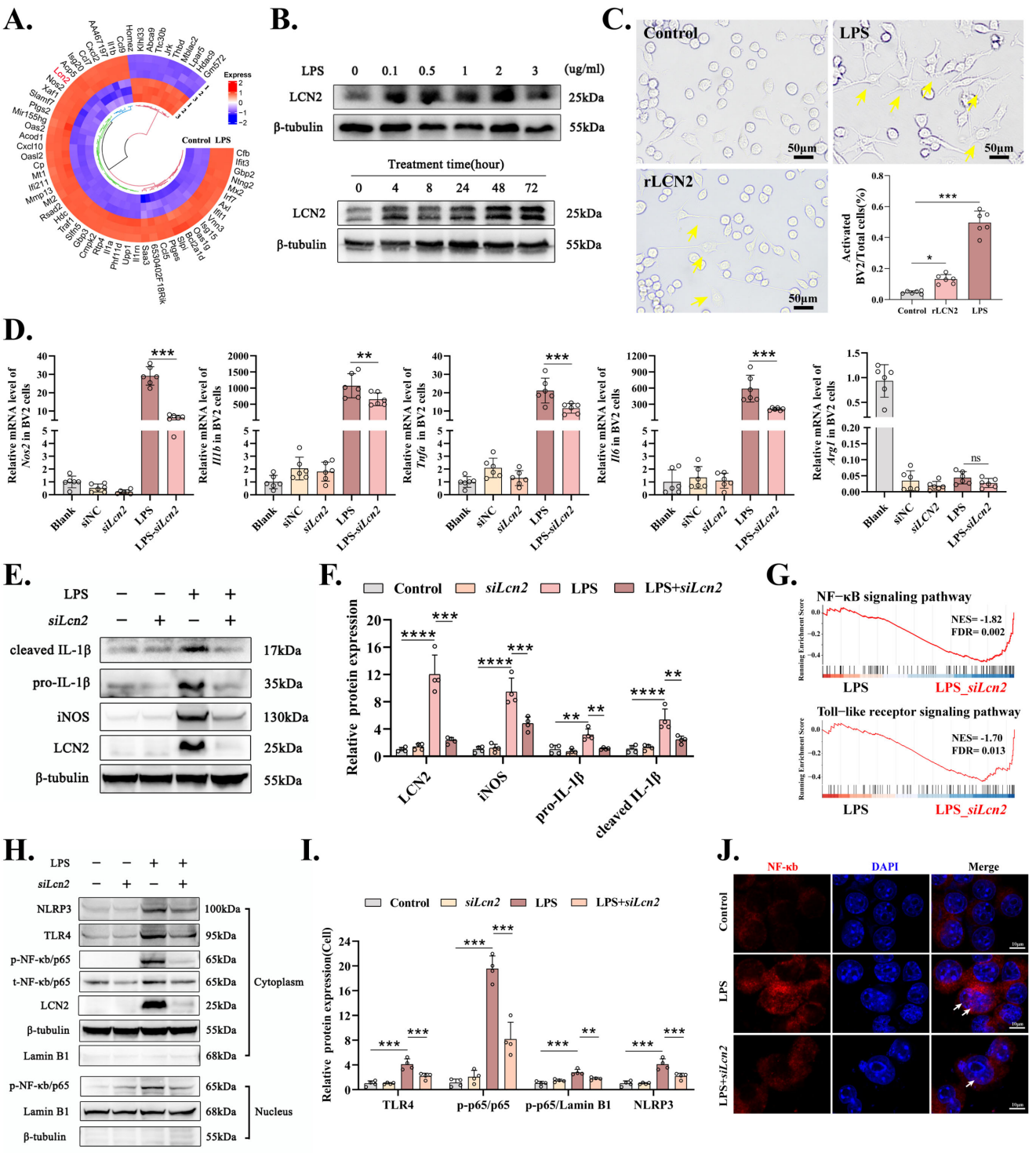

Figure 8. LCN2 knockdown attenuates the inflammatory response by suppressing NLRP3 inflammasome activation through the TLR4/NF-κL pathway. (**A**) Heatmap depicting the differential gene expression between the control and LPS (1 µg/mL) treated groups in BV2 cells based on bulk RNA-seq. (**B**) Immunoblot analysis of LCN2 levels in BV2 cells treated with varying concentrations of LPS (0–3 µg/mL) and exposed to 1 µg/mL LPS for 1 to 3 days. (**C**) Representative microscopy images of resting and activated microglia following LPS treatment. Increased presence of activated microglia exhibiting a ramified morphology and enlarged soma (indicated by *yellow arrowheads*) observed after treatment with rLCN2 for 24 hours. Data are shown as mean ± SEM with $n = 6$. $^{*}P < 0.05$, $^{***}P < 0.001$, calculated by one-way ANOVA. *Scale bar*: 50 µm. (**D**) mRNA expression of proinflammatory cytokines secreted by microglia in vitro after treatment with LPS and/or si*LCN2* measured via RT-qPCR. Gene expressions were normalized to *Gapdh*. Data are presented as mean ± SEM with $n = 6$. $^{*}P < 0.05$, $^{***}P < 0.001$, calculated using one-way ANOVA. (**E**, **F**) Immunoblot analysis of iNOS, pro–IL-1β, cleaved IL-1β, and LCN2 in BV2 cells treated with LPS (1 µg/mL) and si*Lcn2*. Data are presented as mean ± SEM with $n = 4$. $^{**}P < 0.01$, $^{***}P < 0.001$, calculated using one-way ANOVA. (**G**) Gene set enrichment analysis profiles of downregulated pathways, including NF-κB and Toll-like receptor signaling pathways, following *Lcn2* knockdown in an LPS-induced environment. (**H**, **I**) Immunoblot detection of NLPR3, TLR4, p-NF-κB, and t-NF-κB in BV2 cells or the nucleus treated with LPS (1 µg/mL) and si*Lcn2*. Data are presented as mean ± SEM with $n = 4$. $^{**}P < 0.01$, $^{***}P < 0.001$, calculated using one-way ANOVA. (**J**) Representative immunofluorescence images of BV2 cells staining with NF-κB showing a decrease in phosphorylated NF-κB in the cell nucleus in the LPS + si*Lcn2* group compared to the LPS group.

sion following ONC. RT-qPCR analysis of the entire retina revealed a significant upregulation of *Lcn2* expression at 12 hours post-ONC ($P < 0.01$), with peak levels observed at 24 hours ($P < 0.001$), as compared to the sham group (Fig. 5A). This finding was further supported by Western blot analysis (Figs. 5B, 5C) and immunohistochemical staining (Figs. 5D, 5E), which demonstrated a marked increase in LCN2 expression at 5 days and 7 days post-ONC compared to the sham group ($P < 0.05$). To determine the cellular localization of increased LCN2 expression, immunofluorescence colocalization studies were performed, revealing LCN2 expression in RGCs as well as in activated microglia and astrocytes at 7 days following ONC (Fig. 5F). This multiparametric characterization establishes LCN2 as a damage-responsive mediator with dual cellular origins (neuronal and glial), exhibiting early transcriptional activation and progressive protein accumulation that parallels neuroinflammatory progression. The spatial association with activated glia suggests LCN2 may orchestrate neuro-glial crosstalk during posttraumatic retinal degeneration.

Proinflammatory and Neurotoxic Effects of LCN2 in the ONC Retina

To investigate LCN2's pathological contributions, intravitreal rLCN2 was administered in both uninjured and ONC-injured retinas. In uninjured eyes, rLCN2 injection did not alter baseline microglial parameters ($Iba1^+$ density: 1.37 ± 0.13 vs. sham 1.00 ± 0.28, $P = 0.28$; $CD68^+/Iba1^+$ ratio: 0.146% ± 0.053% vs. sham 0.167% ± 0.039%, $P = 0.95$). However, in ONC-injured retinas, rLCN2 significantly exacerbated microglial activation, increasing $Iba1^+$ density by 38.8% ($P < 0.05$ vs. ONC + PBS) and $CD68^+/Iba1^+$ ratio by 35.8% ($P < 0.05$ vs. ONC + PBS; Figs. 6A–C).

RT-qPCR analysis revealed that ONC injury induced significant upregulation of microglial-associated inflammatory mediators (*Fcgr3*, *Tnfa*, *Il1b*, and *Il6*), which was further amplified by rLCN2 coadministration (Fig. 6D). Neuronal viability assessment demonstrated LCN2's context-dependent neurotoxicity: while rLCN2 alone showed no effect on uninjured RGCs (94.5% ± 3.9% vs. sham 100.0% ± 5.4%, $P = 0.25$), it accelerated ONC-induced RGC loss (28.5% ± 5.7% survival in ONC + PBS vs. 37.9% ± 1.4% in ONC + rLCN2, $P < 0.05$; Figs. 6E, 6F).

Mechanistically, daily 4PBA treatment suppressed ONC-induced LCN2 protein expression versus PBS controls ($P < 0.05$; Figs. 6G, 6H). These data establish LCN2 as both a mediator and an amplifier of neuroinflammation through microglial activation and phenotypic switching, with 4PBA-mediated retinal protection involving suppression of this pathogenic axis.

AAV-Mediated LCN2 Gene Silencing Mitigates Microglial Activation and Confers Robust RGC Neuroprotection Post-ONC

Building on evidence of LCN2's pathogenic role, we next employed AAV-mediated gene silencing to therapeutically target LCN2. To assess transfection efficiency, retinal whole mounts were immunostained for EGFP combined with RBPMS (RGC marker) and Iba1 (microglial marker) 3 weeks after intravitreal injection of AAV2-U6-shLcn2-CMV-EGFP (AAV-*Lcn2*). EGFP fluorescence colocalized with both $RBPMS^+$ RGCs and $Iba1^+$ microglia, confirming successful transfection in these cell populations (Figs. 7A, 7B). Western blot analysis further validated a significant reduction in LCN2 protein levels in ONC + AAV-*Lcn2* retinas compared to ONC + AAV-*null* controls ($P < 0.001$; Fig. 7C).

In ONC-injured retinas, AAV-*Lcn2* treatment reduced microglial density by 35.2% ($P < 0.001$), accompanied by a morphologic shift from amoeboid to ramified states (Figs. 7D, 7E). Concurrently, *Lcn2* knockdown enhanced RGC survival to 53.5% ± 3.1% in ONC-injured retinas, significantly surpassing both AAV-null controls (40.5% ± 2.8%, $P < 0.001$) and the ER stress inhibitor 4PBA in parallel experiments (Figs. 7F, 7G). These findings establish *Lcn2* silencing as a precision therapeutic strategy that attenuates microglial-driven neuroinflammation and rescues RGC loss with greater efficacy than broad-spectrum ER stress inhibition, providing a mechanistic rationale for LCN2-targeted interventions in traumatic optic neuropathies.

Lcn2 Ablation Reduces Inflammatory Response by Inhibiting NLRP3 Inflammasome Activation Through the TLR4/NF-κB Pathway In Vitro

To delineate LCN2's regulatory role in inflammatory cascades, we established an LPS-activated BV2 microglial model (1 µg/mL, 24 hours). Bulk RNA-seq analysis revealed significant *Lcn2* upregulation in LPS-treated cells versus controls (Fig. 8A), corroborated by immunoblot showing dose- and time-dependent LCN2 protein induction (Fig. 8B). Morphologic analysis demonstrated that both LPS and rLCN2 triggered microglial activation, with pseudopodia-rich amoeboid cells significantly increasing versus PBS controls ($P < 0.05$; Fig. 8C).

siRNA-mediated *Lcn2* silencing attenuated LPS-driven proinflammatory responses, downregulating *Il1b*, *Nos2*, *Tnfa*, and *Il6* mRNA levels ($P < 0.05$; Fig. 8D), paralleled by reduced pro–IL-1β, cleaved IL-1β, and iNOS protein expression ($P < 0.01$; Figs. 8E, 8F). Gene set enrichment analysis identified suppressed TLR4/NF-κB signaling ($NES = -1.70$, $FDR < 0.05$) following *Lcn2* knockdown (Fig. 8G), validated by immunoblot showing si*Lcn2*-mediated reversal of LPS-induced TLR4 upregulation and NF-κB phosphorylation (Figs. 8H, 8I), with immunofluorescence confirming diminished nuclear p-NF-κB translocation (Fig. 8J). Given that the NF-κB pathway is a key regulator of NLRP3 inflammasome activation,[30] we also assessed the role of LCN2 in inflammasome activation. Our findings demonstrated that LPS-induced NLRP3 inflammasome activation was inhibited by siLcn2 treatment (Figs. 8H, 8I). Overall, our findings highlight the significant role of LCN2 in the activation of microglial cells toward a proinflammatory phenotype through the TLR4/NF-κB pathway by activating the NLRP3 inflammasome.

In summary, these data indicate that ER stress exacerbates post-ONC retinal degeneration via LCN2-dependent microglial reprogramming. Therapeutic targeting of this axis through pharmacologic ER stress inhibition or genetic *Lcn2* silencing attenuates neuroinflammation by suppressing TLR4/NF-κB–driven NLRP3 inflammasome activation, highlighting LCN2 as a pivotal mediator bridging metabolic stress with innate immune activation in optic neuropathies.

Investigative Ophthalmology & Visual Science

Discussion

This study delineates a pathogenic axis linking ER stress with neuroinflammation through LCN2-mediated microglial reprogramming in posttraumatic retinal degeneration. We demonstrate that ONC triggers ER stress activation—an acute unfolded protein response (UPR) response within 4 hours followed by sustained *Ddit3* (CHOP)*/Hspa5* (GRP78) elevation persisting through day 7. Pharmacologic ER stress inhibition via 4PBA conferred neuroprotection by attenuating microglial activation, while genetic *Lcn2* silencing achieved superior RGC preservation through targeted disruption of the TLR4/NF-κB cascade and NLRP3 inflammasome signaling. Our findings position LCN2 as a key molecular connecting ER stress with innate immune activation in optic neuropathies.

ER Stress Dynamics in Posttraumatic Retinal Degeneration

ER stress triggers the UPR, activating adaptive mechanisms for protein folding, quality control, and degradation or leading to apoptosis if damage is irreversible.[31] Notably, ER stress is recognized as a critical proapoptotic pathway involved in RGC death following injury.[10,11] Our temporal profiling revealed early-phase UPR activation (*Atf4/Ddit3* [CHOP] induction at 4 hours) preceding morphologic RGC degeneration, suggesting ER stress initiates rather than merely accompanies neuronal loss. This aligns with the demonstration by Hu et al.[13] of CHOP-mediated apoptosis in axon injury–induced models, yet extends these observations by documenting sustained ER stress burden through day 7 post-ONC—a critical period for secondary degeneration. The microglial-specific GRP78 upregulation at day 3 post-ONC suggests non-cell-autonomous ER stress propagation—a phenomenon increasingly recognized in neuroinflammatory cascades.[32,33] ER stress responses in surrounding neuroglia can enhance disease progression by coordinating damaging inflammatory responses that create a neurotoxic environment.[15] In this study, 4PBA administration significantly suppressed ONC-induced ER stress potentially via the ATF4-CHOP signaling pathway. In addition to inhibiting ER stress, 4PBA treatment mitigated retinal damage characterized by RGC loss and retinal layer thinning. Neuroinflammation, evidenced by microglial activation and increased inflammatory molecules after ONC, was also reduced by 4PBA treatment. The neuroprotective and anti-inflammatory effects of 4PBA are consistent with findings in various other disease models.[34–36] However, the modest improvement of 4PBA in RGC survival following ONC despite ER stress suppression highlights critical limitations: (1) ER stress exhibits dual roles in RGC survival—while excessive stress drives apoptosis, moderate stress activates adaptive XBP1-mediated survival pathways[13,37] that may be compromised by 4PBA, and (2) multifactorial RGC degeneration mechanisms (e.g., metabolic disorders and dysregulated glial responses) persist beyond ER stress modulation.[38] Given these limitations, current approaches utilizing broad ER stress inhibitors, such as 4PBA, demonstrate limited therapeutic potential. To achieve better outcomes, more precise intervention strategies are necessary. Targeting the pathological interplay between ER stress and neuroinflammation could be a more effective intervention strategy, as this interplay is a key driver of neuronal degeneration.

ER Stress Participates in LPS-Induced Inflammation Regulation

ER stress, often associated with inflammation, has been shown to modulate inflammatory and immune responses in various diseases.[39–41] Converging evidence reveals that severe ER stress initiates UPR-dependent inflammatory cascades via interconnected mechanisms: calcium efflux from ER stores, NF-κB activation, and acute-phase response induction, collectively driving cytokine/chemokine overproduction and oxidative stress.[30,42–44] To dissect this complexity, we employed LPS as a dual-function stimulus—activating both TLR4-mediated inflammation and ER stress through distinct mechanisms. Beyond its canonical TLR4 signaling, LPS directly triggers ER stress via calcium dysregulation (PERK-ATF4-CHOP axis) and reactive oxygen species (ROS)–dependent UPR activation (IRE1α-XBP1 pathway).[29,45] This dual activity enabled targeted investigation of ER stress contributions using 4PBA, a chemical chaperone that suppresses ER stress. Notably, 4PBA attenuated LPS-driven neuroinflammation in our BV2 microglia model, aligning with its efficacy in the acute lung injury model.[45] Importantly, we identified LCN2 as the critical molecular bridge linking ER stress with inflammatory amplification—a finding with broad implications for neuroinflammatory diseases.

LCN2 as a Bidirectional Mediator of ER Stress–Inflammation Crosstalk

Mechanistically, LCN2 emerged as a feedforward amplifier of ER stress–microglial activation. The reciprocal regulation observed in BV2 cells—where TUN-induced ER stress upregulated LCN2, and *Lcn2* silencing attenuated CHOP/GRP78 expression—establishes a self-reinforcing loop perpetuating neuroinflammation. This regulatory synergy, previously characterized in kidney[23] and pulmonary[21] systems through iron dysregulation, acquires unique significance in neural contexts where LCN2's spatiotemporal expression mirrors degenerative progression. Our LPS costimulation model further confirmed LCN2's dual regulatory capacity, as silencing concurrently dampened ER stress markers and proinflammatory mediators. Despite its recognized role as an acute-phase protein,[46,47] LCN2's functional duality in CNS pathologies remains debated: while some studies suggest neuroprotective roles in systemic inflammation,[48] accumulating evidence indicates its pathogenic promotion of microglial/astrocyte activation in local neuroinflammation and contributing to neuronal injury.[49–51] In our ONC model, LCN2 upregulation in activated glia correlated with exacerbated RGC loss, exhibiting context-dependent neurotoxicity requiring preexisting injury milieus, likely through cooperation with damage-associated molecular patterns (e.g., ROS, ATP) that prime microglial responsiveness. These findings align with emerging concepts of "context-dependent glial plasticity."[52] *Lcn2* silencing as a precision therapeutic strategy attenuates microglial-driven neuroinflammation and rescues RGC loss with greater efficacy than broad-spectrum ER stress inhibition, providing a mechanistic rationale for LCN2-targeted interventions in traumatic optic neuropathies. The mechanistic dissection of LCN2's TLR4/NF-κB/NLRP3 signaling axis provides a rationale for its superior neuroprotection. Previous studies have reported that ER stress can trigger inflammation through the NLRP3 inflammasome.[53] Notably, NLRP3 is involved in various forms of RGC death,

including pyroptosis, apoptosis, necrosis, ferroptosis, and PANoptosis, suggesting that ER stress may mediate RGC loss via NLRP3 activation.[39] This aligns with our findings that the ER stress inhibitor 4PBA can suppress LCN2 expression and exert anti-neuroinflammatory and neuroprotective effects, potentially by inhibiting NLRP3 inflammasome activation through the TLR4/NF-κB pathway following ONC.

Limitations and Future Directions

It is important to recognize that the use of contralateral eyes as controls, although validated in acute-phase experiments (Supplementary Fig. S1), has inherent limitations. While no significant differences were observed between contralateral and naive blank controls in RGC survival or microglial density during the acute phase, contralateral eyes may still experience systemic or compensatory neuroinflammatory crosstalk in an experimental glaucoma model.[54] This design choice, although supported by methodologic precedents,[26,27] prevents us from definitively excluding bilateral signaling effects that could influence long-term outcomes. Furthermore, this study focused on retinal changes postinjury, leaving the role of LCN2 in the optic nerve itself unexplored—a critical area for future investigation.

Conclusions

This study establishes LCN2 as a key mediator linking ER stress with neuroinflammation in optic nerve injury (Fig. 9). By elucidating the TLR4/NF-κB/NLRP3 signaling axis, we demonstrate that LCN2-targeted gene therapies achieve greater specificity and efficacy compared to broad ER stress inhibition. These findings position LCN2 as a promising therapeutic target, offering a novel approach to disrupt the pathological interplay between ER stress and inflammation, thereby enhancing treatment strategies for optic neuropathies.

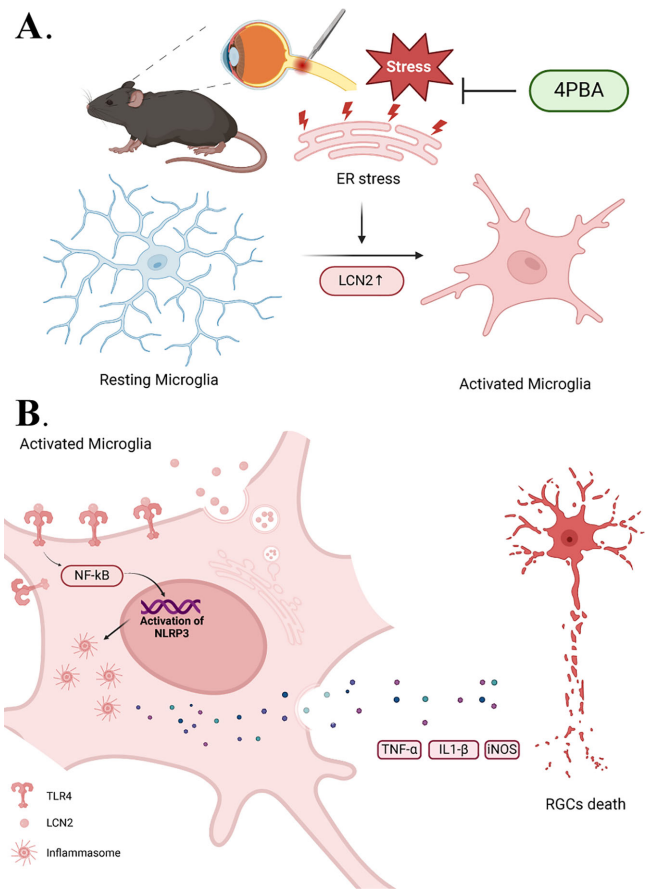

Figure 9. Schematic illustrating the proposed molecular mechanism by which LCN2 connects ER stress and inflammation following optic nerve injury.

Acknowledgments

Supported by the Natural Science Foundation of China (82471068), the Guangzhou Basic Research Program Joint Funding Project for Schools (Institutes) (2023A3J0179), and the Natural Science Foundation of Guangdong Province (2023A1515010532).

Data supporting the findings of this study are available upon reasonable request to the corresponding author.

Disclosure: **W. Huang**, None; **Y. Liu**, None; **J. Li**, None; **Y. Gao**, None; **J. Tang**, None; **S. Yip**, None; **X. Wang**, None; **H. Zhang**, None; **Y. Ma**, None; **S. Su**, None; **J. Nie**, None; **R. Lu**, None

References

1. Peng J, Jin J, Su W, et al. High-mobility group box 1 inhibitor boxA alleviates neuroinflammation-induced retinal ganglion cell damage in traumatic optic neuropathy. *Int J Mol Sci*. 2022;23(12):6715.
2. Fang F, Liu P, Huang H, et al. RGC-specific ATF4 and/or CHOP deletion rescues glaucomatous neurodegeneration and visual function. *Mol Ther Nucleic Acids*. 2023;33:286–295.
3. Au NPB, Ma CHE. Neuroinflammation, microglia and implications for retinal ganglion cell survival and axon regeneration in traumatic optic neuropathy. *Front Immunol*. 2022;13:860070.
4. Rathnasamy G, Foulds WS, Ling EA, Kaur C. Retinal microglia—a key player in healthy and diseased retina. *Prog Neurobiol*. 2019;173:18–40.
5. Zhang SX, Wang JJ, Starr CR, et al. The endoplasmic reticulum: homeostasis and crosstalk in retinal health and disease. *Prog Retin Eye Res*. 2024;98:101231.
6. Liu N, Bai L, Lu Z, et al. TRPV4 contributes to ER stress and inflammation: implications for Parkinson's disease. *J Neuroinflammation*. 2022;19(1):26.
7. Ajoolabady A, Lindholm D, Ren J, Pratico D. ER stress and UPR in Alzheimer's disease: mechanisms, pathogenesis, treatments. *Cell Death Dis*. 2022;13(8):706.
8. De Lorenzo F, Lüningschrör P, Nam J, et al. CDNF rescues motor neurons in models of amyotrophic lateral sclerosis by targeting endoplasmic reticulum stress. *Brain*. 2023;146(9):3783–3799.
9. Kasetti RB, Patel PD, Maddineni P, et al. ATF4 leads to glaucoma by promoting protein synthesis and ER client protein load. *Nat Commun*. 2020;11(1):5594.
10. Syc-Mazurek SB, Fernandes KA, Wilson MP, Shrager P, Libby RT. Together JUN and DDIT3 (CHOP) control retinal ganglion cell death after axonal injury. *Mol Neurodegener*. 2017;12(1):71.
11. Tian F, Cheng Y, Zhou S, et al. Core transcription programs controlling injury-induced neurodegeneration of retinal ganglion cells. *Neuron*. 2022;110(16):2607–2624.e8.
12. Bilbao-Malavé V, González-Zamora J, de la Puente M, et al. Mitochondrial dysfunction and endoplasmic reticulum stress in age related macular degeneration, role in patho-

physiology, and possible new therapeutic strategies. *Antioxidants (Basel)*. 2021;10(8):1170.
13. Hu Y, Park KK, Yang L, et al. Differential effects of unfolded protein response pathways on axon injury-induced death of retinal ganglion cells. *Neuron*. 2012;73(3):445–452.
14. Reverendo M, Mendes A, Argüello RJ, Gatti E, Pierre P. At the crossway of ER-stress and proinflammatory responses. *FEBS J*. 2019;286(2):297–310.
15. Sprenkle NT, Sims SG, Sánchez CL, Meares GP. Endoplasmic reticulum stress and inflammation in the central nervous system. *Mol Neurodegener*. 2017;12(1):42.
16. Liu T, Li T, Chen X, et al. EETs/sEHi alleviates nociception by blocking the crosslink between endoplasmic reticulum stress and neuroinflammation in a central poststroke pain model. *J Neuroinflammation*. 2021;18(1):211.
17. Jung BK, Park Y, Yoon B, et al. Reduced secretion of LCN2 (lipocalin 2) from reactive astrocytes through autophagic and proteasomal regulation alleviates inflammatory stress and neuronal damage. *Autophagy*. 2023;19(8):2296–2317.
18. Jung BK, Ryu KY. Lipocalin-2: a therapeutic target to overcome neurodegenerative diseases by regulating reactive astrogliosis. *Exp Mol Med*. 2023;55(10):2138–2146.
19. Yao SQ, Wang M, Liang JJ, Ng TK, Cen LP. Retinal transcriptome of neonatal mice after optic nerve injury. *PLoS One*. 2023;18(5):e0286344.
20. Ueno S, Yoneshige A, Koriyama Y, Hagiyama M, Shimomura Y, Ito A. Early gene expression profile in retinal ganglion cell layer after optic nerve crush in mice. *Invest Ophthalmol Vis Sci*. 2018;59(1):370–380.
21. Wang G, Liu S, Wang L, et al. Lipocalin-2 promotes endoplasmic reticulum stress and proliferation by augmenting intracellular iron in human pulmonary arterial smooth muscle cells. *Int J Biol Sci*. 2017;13(2):135–144.
22. Chan YK, Sung HK, Sweeney G. Iron metabolism and regulation by neutrophil gelatinase-associated lipocalin in cardiomyopathy. *Clin Sci (Lond)*. 2015;129(10):851–862.
23. El Karoui K, Viau A, Dellis O, et al. Endoplasmic reticulum stress drives proteinuria-induced kidney lesions via Lipocalin 2. *Nat Commun*. 2016;7:10330.
24. Smith HL, Freeman OJ, Butcher AJ, et al. Astrocyte unfolded protein response induces a specific reactivity state that causes non-cell-autonomous neuronal degeneration. *Neuron*. 2020;105(5):855–866.e5.
25. Yao K, Mou Q, Lou X, et al. Microglial SIRT1 activation attenuates synapse loss in retinal inner plexiform layer via mTORC1 inhibition. *J Neuroinflammation*. 2023;20(1):202.
26. Wang J, He X, Meng H, et al. Robust myelination of regenerated axons induced by combined manipulations of GPR17 and microglia. *Neuron*. 2020;108(5):876–886.e4.
27. Lin S, Gao W, Zhu C, et al. Efficiently suppress of ferroptosis using deferoxamine nanoparticles as a new method for retinal ganglion cell protection after traumatic optic neuropathy. *Biomater Adv*. 2022;138:212936.
28. Tang J, Liu Y, Zhang Z, et al. Heterogeneous expression patterns of the minichromosome maintenance complex members in retinoblastoma unveil its clinical significance. *Invest Ophthalmol Vis Sci*. 2024;65(1):31.
29. Kim HJ, Kim DH, Park W. Moutan cortex extract modulates macrophage activation via lipopolysaccharide-induced calcium signaling and ER stress-CHOP pathway. *Int J Mol Sci*. 2023;24(3):2062.
30. Li W, Cao T, Luo C, et al. Crosstalk between ER stress, NLRP3 inflammasome, and inflammation. *Appl Microbiol Biotechnol*. 2020;104(14):6129–6140.
31. Hetz C, Saxena S. ER stress and the unfolded protein response in neurodegeneration. *Nat Rev Neurol*. 2017;13(8):477–491.
32. Guo M, Wang J, Zhao Y, et al. Microglial exosomes facilitate α-synuclein transmission in Parkinson's disease. *Brain*. 2020;143(5):1476–1497.
33. Sarkar S. Microglial ion channels: key players in non-cell autonomous neurodegeneration. *Neurobiol Dis*. 2022;174:105861.
34. Huang Y, Yuan M, Duan F, Yang Y, Lou B, Lin X. Inhibition of endoplasmic reticulum stress by 4–phenylbutyrate alleviates retinal inflammation and the apoptosis of retinal ganglion cells after ocular alkali burn in mice. *Inflamm Res*. 2022;71(5–6):577–590.
35. Tiwari S, Gupta P, Singh A, et al. 4-Phenylbutyrate mitigates the motor impairment and dopaminergic neuronal death during Parkinson's disease pathology via targeting VDAC1 mediated mitochondrial function and astrocytes activation. *Neurochem Res*. 2022;47(11):3385–3401.
36. Zode GS, Bugge KE, Mohan K, et al. Topical ocular sodium 4-phenylbutyrate rescues glaucoma in a myocilin mouse model of primary open-angle glaucoma. *Invest Ophthalmol Vis Sci*. 2012;53(3):1557–1565.
37. Huang H, Miao L, Liang F, et al. Neuroprotection by eIF2α-CHOP inhibition and XBP-1 activation in EAE/optic neuritiss. *Cell Death Dis*. 2017;8(7):e2936.
38. Li Y, Andereggen L, Yuki K, et al. Mobile zinc increases rapidly in the retina after optic nerve injury and regulates ganglion cell survival and optic nerve regeneration. *Proc Natl Acad Sci USA*. 2017;114(2):E209–E218.
39. Chen X, Shi C, He M, Xiong S, Xia X. Endoplasmic reticulum stress: molecular mechanism and therapeutic targets. *Signal Transduct Target Ther*. 2023;8(1):352.
40. Zhang Y, Chen W, Wang Y. STING is an essential regulator of heart inflammation and fibrosis in mice with pathological cardiac hypertrophy via endoplasmic reticulum (ER) stress. *Biomed Pharmacother*. 2020;125:110022.
41. Ajoolabady A, Lebeaupin C, Wu NN, Kaufman RJ, Ren J. ER stress and inflammation crosstalk in obesity. *Med Res Rev*. 2023;43(1):5–30.
42. Ooi K, Hu L, Feng Y, et al. Sigma-1 receptor activation suppresses microglia M1 polarization via regulating endoplasmic reticulum-mitochondria contact and mitochondrial functions in stress-induced hypertension rats. *Mol Neurobiol*. 2021;58(12):6625–6646.
43. Wang X, Li S, Yu J, et al. Saikosaponin B2 ameliorates depression-induced microglia activation by inhibiting ferroptosis-mediated neuroinflammation and ER stress. *J Ethnopharmacol*. 2023;316:116729.
44. Kitamura M. Control of NF-κB and inflammation by the unfolded protein response. *Int Rev Immunol*. 2011;30(1):4–15.
45. Zeng M, Sang W, Chen S, et al. 4-PBA inhibits LPS-induced inflammation through regulating ER stress and autophagy in acute lung injury models. *Toxicol Lett*. 2017;271:26–37.
46. Lee S, Lee J, Kim S, et al. A dual role of lipocalin 2 in the apoptosis and deramification of activated microglia. *J Immunol*. 2007;179(5):3231–3241.
47. Lee S, Kim JH, Kim JH, et al. Lipocalin-2 is a chemokine inducer in the central nervous system: role of chemokine ligand 10 (CXCL10) in lipocalin-2-induced cell migration. *J Biol Chem*. 2011;286(51):43855–43870.
48. Kang SS, Ren Y, Liu CC, et al. Lipocalin-2 protects the brain during inflammatory conditions. *Mol Psychiatry*. 2018;23(2):344–350.
49. Rathore KI, Berard JL, Redensek A, et al. Lipocalin 2 plays an immunomodulatory role and has detrimental effects after spinal cord injury. *J Neurosci*. 2011;31(38):13412–13419.
50. Kim JH, Kang RJ, Hyeon SJ, et al. Lipocalin-2 is a key regulator of neuroinflammation in secondary traumatic and ischemic brain injury. *Neurotherapeutics*. 2023;20(3):803–821.

Investigative Ophthalmology & Visual Science

51. Jiang SY, Tian T, Yao H, et al. The cGAS-STING-YY1 axis accelerates progression of neurodegeneration in a mouse model of Parkinson's disease via LCN2-dependent astrocyte senescence. *Cell Death Differ*. 2023;30(10):2280–2292.
52. Augusto-Oliveira M, Arrifano GP, Delage CI, Tremblay MÈ, Crespo-Lopez ME, Verkhratsky A. Plasticity of microglia. *Biol Rev Camb Philos Soc*. 2022;97(1):217–250.
53. Bronner DN, Abuaita BH, Chen X, et al. Endoplasmic reticulum stress activates the inflammasome via NLRP3- and caspase-2-driven mitochondrial damage. *Immunity*. 2015;43(3):451–462.
54. Tribble JR, Kokkali E, Otmani A, et al. When is a control not a control? Reactive microglia occur throughout the control contralateral pathway of retinal ganglion cell projections in experimental glaucoma. *Transl Vis Sci Technol*. 2021;10(1):22.

Investigative Ophthalmology & Visual Science